# Pressure Feedback Technique to improve performance of a Supersonic Air Intake at Mach 2.2

This study presents a comprehensive computational investigation of a supersonic mixed compression air intake modified using the Pressure Feedback Technique (PFT) to enhance startability and performance at a design Mach number of 2.2 with zero-degree cowl deflection. Four different configurations, referred to as M1, M2, M3, and M4, were analysed and compared with a baseline model. The influence of PFT on shock structures, flow separation, and pressure distribution within the intake was systematically evaluated using Mach number and velocity contours, density plots, and streamline visualizations. RANS equations are solved using k-omega SST turbulence model in the Ansys CFD package software. Results showed that cases M3 and M4 achieved a complete start condition, characterized by fully developed shock reflections and improved internal flow behaviour. Case M2 demonstrated a near-started condition with controlled bow shock behaviour and minimal flow spillage, while M1 remained in an unstarted state but exhibited reduced flow distortion. Quantitative performance metrics, including Total Pressure Recovery (TPR) and Flow Distortion (FD), were assessed using standard formulations. Overall, the study validates the effectiveness of the Pressure Feedback Technique as a passive control strategy for improving the operability and efficiency of supersonic air intake systems under challenging flow

**Keywords:** Supersonic air intake, Starting Behaviour, SWBLI control, Performance Parameters.

#### Sorabh Khurana

PhD-Student Department of Mechanical Engineering National Institute of Technology Kurukshetra, Haryana India

#### Neeraj Kumar Gahlot

Assistant Professor-III
Amity Institute of Aerospace Engineering
Amity University Uttar Pradesh, Noida
India-201313

#### **Nirmal Kant Singh**

conditions.

Associate Professor Department of Mechanical Engineering National Institute of Technology Kurukshetra, Haryana India

#### 1. INTRODUCTION

Air intakes in air-breathing propulsion systems serve the crucial function of capturing atmospheric air and delivering it to the engine to generate the required thrust, as well as to the onboard conditioning systems. In high-speed flight, intakes also perform the role of a compressor [1] by decelerating the high Mach number free-stream airflow, and increasing its pressure before it enters the engine. The primary objective in designing a supersonic intake is to ensure that it meets the aerodynamic performance needed for the mission [2]. Key performance criteria include achieving high total pressure recovery to maximize engine thrust, maintaining low flow distortion for stable compressor operation, and providing robustness against transient variations in free-stream Mach number, angle of attack, and engine flow demands to ensure safety [3]. Air intake performance are severely affected by shock wave boundary layer interaction (SWBLI) [4]. It's an unwanted feature of supersonic aerodynamics. It occurs when a shock wave strikes a surface already sheathed in a boundary layer, spawning secondary shocks within

Received: August 2025, Accepted: September 2025 Correspondence to: Dr Neeraj Kumar Gahlot, Assistant Professor-III, Amity Institute of Aerospace Engineering Amity University Uttar Pradesh, Noida, India-201313 E-mail: neerajkumargahlot@gmail.com

doi: 10.5937/fme2504595K

that viscous layer [5]. The interaction zone experiences a sharp pressure rise that imposes a severe adverse pressure gradient, thickening the boundary layer and often forcing it to separate and form a separation bubble[6]. This bubble diminishes mass-flow capture, degrades total-pressure recovery, and reduces overall intake efficiency. In addition, SWBLI can introduce large-scale unsteadiness, such as intake buzz [7] and oscillatory side loads, that portends the stability and structural integrity of the intake system. Increased drag and elevated local heating are additional adverse effects associated with SWBLI. These phenomena can ultimately cause the intake to unstart [8], a condition where stable airflow into the engine is disrupted. The turbulence generated during SWBLI enhances viscous dissipation, further increasing drag and reducing the engine's overall efficiency. When shock-induced separation occurs in a supersonic inlet, it creates extensive regions of separated flow accompanied by vortices [9], contributing to greater flow unsteadiness and higher acoustic loading. Moreover, SWBLI intensifies aerodynamic contraction, and if this contraction surpasses the critical threshold defined by Kantrowitz's limit [10], inlet unstart becomes inevitable. Collectively, these effects degrade the performance of the air intake system and pose risks to its structural and operational integrity

Improving intake performance by mitigating the intensity of SWBLI in high-speed air-breathing systems remains an active and ongoing area of investigation.

Numerous studies and experimental efforts have been documented in the literature over the years, reflecting sustained interest in enhancing the aerodynamic efficiency and stability of such propulsion systems. Emami et al. [11] conducted an extensive experimental study using a combination of interchangeable, rotating cowls of varying lengths and isolator sections of different dimensions. Start and unstart behaviour was analysed through static pressure measurements taken along the ramp and cowl surfaces. The experiments revealed that inlet unstart consistently occurred at nearly the same cowl convergence angle, regardless of the cowl length. However, unstart induced by back pressure from the combustor was found to depend on factors such as inlet geometry, contraction ratio, and isolator length. Later, Janarthanam and Babu [12] carried out a computational study replicating Emami's intake geometry and experimental conditions. They analyzed three different cowl lengths and five cowl convergence angles. Their findings confirmed that intake unstart is primarily a downstream consequence of SWBLI within the intake. In particular, the location where the shock impinges on the ramp shoulder was identified as a critical factor influencing flow distortion at the entry of the isolator, which in turn affects intake stability. Continuing, Das and Prasad [13] revisited the mixedcompression intake originally introduced by Neale and Lamb [14]. Through a combined experimental-numerical study, they examined how cowl-deflection angle, boundary-layer bleed, and angle of incidence influence the internal shock structure and, in turn, the starting and unstart behavior of the intake. Among these parameters, the cowl-deflection angle proved most critical, as it dictated the size of the separation zone near the throat and at the site of the strongest shock boundary layer interaction. Jayanta et al. [15] carried out a comprehensive study to investigate the influence of Mach number and angle of attack on the performance of a supersonic air intake system. In their work, a multipleramp diverterless intake (MRD) configuration was employed to enhance overall intake efficiency by minimizing flow distortions and improving pressure recovery. The study systematically analyzed intake behavior across a wide range of Mach numbers and operating conditions, demonstrating that the MRD approach offers superior mass capture and stability compared to conventional intake designs. Mahapatra and Jagadeesh [16] experimentally investigated the impact of varying contraction ratios in a two-dimensional planar intake designed for Mach 8. At higher contraction ratios, they documented regular shock reflections, the formation of a substantial separation zone near the shoulder. In contrast, lower contraction ratios produced a markedly reduced separation region. Numerous additional studies, such as those by Murugan et al. [17] and Erdem et al. [18] likewise explore scramjet-intake design. Across this work, boundary-layer separation arising from the interaction of the cowl-lip shock with the boundary layer on the ramp wall consistently appears as the dominant mechanism degrading intake performance.

Numerous studies have focused on mitigating SWBLI and its associated adverse effects, particularly the formation of separation bubbles, which degrade in-

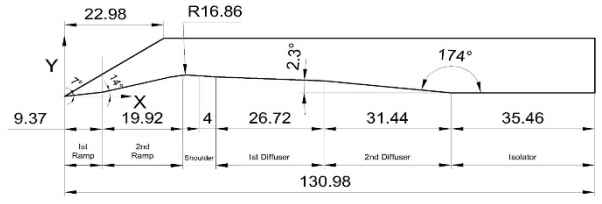
take performance in high-speed air-breathing engines. Both active and passive flow control strategies have been explored to suppress or delay boundary layer separation and improve total pressure recovery. Active flow control techniques, which involve external energy or control input, offer dynamic adaptability and potentially higher effectiveness. For example, plasma actuators [19] can locally modify the boundary layer properties to prevent or reduce separation during SWBLI. The use of localized heat sources [20] is another active method that introduces thermal energy to locally reduce air density and viscosity gradients, which can manipulate the boundary layer thickness and influence the shock interaction zone. These thermal effects can smooth the pressure gradients and suppress separation if properly controlled. While active techniques offer more flexibility, their integration into high-speed propulsion systems remains complex due to energy requirements and system-level implications. On the other hand, Passive techniques [21], which require no external energy input, are widely used due to their simplicity and robustness. Among these, vortex generators (VGs) are a common solution that introduce streamwise vortices to energize the boundary layer and delay separation by enhancing momentum exchange across the shear layer [22]. Surface bleed [23] is another effective passive tec hnique, wherein a portion of the low-energy boundary layer is removed through porous surfaces or slots, thereby reducing the interaction strength and weakening the separation. Wall bifurcations and cavities [24] have also been explored to alter the shock structure and redistribute pressure gradients in a way that mitigates SWBLI. For instance, cavities upstream of the interaction zone have been shown to trap and stabilize the separated region, thereby minimizing unsteady effect. Additionally, backward-facing steps [25] can be strategically placed to induce flow reattachment and disrupt adverse pressure buildup before it interacts with the boundary layer. Gahlot and Singh [26] recently investigated the impact of cowl ventilation on the starting behaviour of a mixed-compression air intake operating under off-design conditions. In their study, four distinct ventilation slots were introduced on the cowl surface, positioned just above the shoulder region of the intake. The incorporation of these ventilation slots significantly altered the shock structure near the throat. Specifically, the strong bow shock typically formed ahead of the throat in the unventilated configuration was completely transformed into a series of oblique shocks. This modification led to improved flow conditions within the intake, indicating that strategic cowl ventilation can effectively enhance starting characteristics and reduce shockinduced flow distortions in mixed-compression intakes. Shogo Ogura et al. [27] investigated the effect of side clearance (SC) on supersonic intake performance at Mach 3.4 through wind tunnel tests. Results showed that the second-ramp SC (upstream of the throat) deteriorates performance, while the third-ramp SC (downstream) improves operability by widening the starting range. A hybrid SC with only the third ramp slit achieved higher mass capture ratio and stable operation but suffered performance loss under sideslip due to additional leakage.

Nevertheless, ongoing research continues to optimize both active and passive strategies, and in some cases, hybrid methods combining the advantages of both have been proposed to achieve greater effectiveness across a broader range of flight conditions. Kulkarni et al.[28][29] have introduced a pressure-feedback technique (PFT) to mitigate the ramp-induced boundary-layer separation that plagues hypersonic vehicles. In their numerical study, they modeled a twodimensional flat-plate/ramp configuration equipped with an internal channel that taps fluid from the adversepressure-gradient region downstream of the ramp and reinjects it farther upstream. Driven solely by the natural pressure difference between the separated pocket and the core flow, this closed-loop "bypass" continuously siphons low-momentum fluid out of the separation bubble and feeds higher-momentum fluid back into the boundary layer. The freestream Mach number, wall temperature ratio, channel cross-section was varied systemically and the precise placement of suction and injection ports to gauge the robustness of the concept. The most effective arrangement positioned the suction slot at the ramp foot, where separation is strongest and the injection slot near the upstream influence point, just ahead of the interaction region. Under these conditions, the PFT shortened the separation bubble length by  $\approx 12$  %, attenuating the severity of the shock-induced adverse pressure gradient without the need for external energy input or moving parts. The Pressure Feedback Technique (PFT) is an innovative, self-regulating flow control method that operates by simultaneously extracting low-energy fluid (suction) and reintroducing it (injection) into the flow, without requiring external energy input. Further Zhong et al.[30] developed and proposed a secondary circulation jet configuration designed for variable Mach number flows. The configuration was examined under inlet Mach numbers of 2.5, 3.0, and 3.5, alongside the introduction of an adaptive control strategy. The analysis indicated that, within the Mach number range of 2.5 to 3.5, the configuration, together with the adaptive control method, contributed significantly to reducing the separation zone volume and total pressure loss. It was also demonstrated that the adaptive control approach could be implemented through passive control methods.

Based on the literature review, researchers have explored the use of Pressure Feedback Techniques (PFT) or similar methods to control SWBLI in corner separations and rectangular ducts. Given the proven effectiveness of such techniques in conventional geometries, it is worthwhile to investigate the application of PFT in conjunction with a mixedcompression supersonic air intake, particularly to address starting issues. In the present study, the authors propose the implementation of PFT to enhance the performance of a supersonic air intake. For this purpose, a modified pressure feedback mechanism has been developed, incorporating four different configurations with varying geometries and shapes. Each configuration consists of a rectangular tube system designed to regulate flow within the supersonic air intake by utilizing internal pressure feedback. In all four cases, one end of the tube is strategically connected to the shoulder region of the air intake, an area where flow separation due to SWBLI is particularly pronounced. The other end of the tube is routed to the various section of the intake. This arrangement facilitates the extraction of high-pressure mass flow from the shoulder or throat region and its re-injection into the downstream section of the air intake. Comprehensive evaluations of the four geometrical (selection of shape, size and inlet-exit locations of tube are explained in next section) tube configurations have been carried out to assess their effectiveness in managing internal flow structures and minimizing total pressure losses. The study demonstrates that such a pressure feedback mechanism can significantly contribute to the robust operation of supersonic air intakes, especially in mixed-compression designs.

#### 2. GEOMETRICAL DETAILS OF THE MODEL

For present investigation, an air intake model having mixed compression with a design Mach number 2.2 at zero-degree cowl deflection is selected, as the experimental data for the same is available to support the computational technique used in this study. Neale and Lamb first suggested this model in 1962[14], while Das and Prasad[1] made a few modifications in 2010 based on the requirements of their wind tunnel facility.



a) Geometric details of the air intake model.

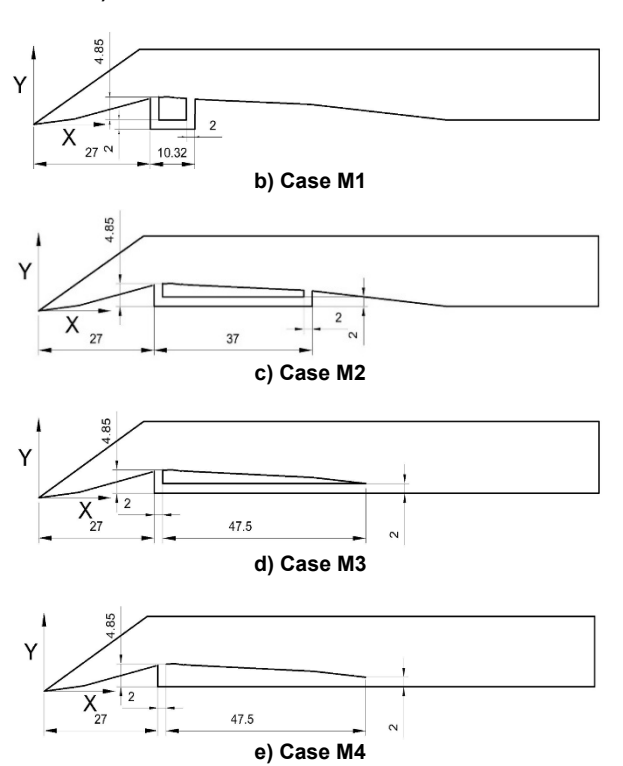


Figure 1. Air intake model dimensions with and without PFT models (mm)

This air intake model features two ramps which are aligned with respect to the direction of the freestream at an angle of 7 and 14 degrees respectively, followed by a throat section and diverging part having 2.3 and 6.0degrees deflection angles. The model's overall length is 130.98 mm, and the air intake height is 15 mm. 2D diagram of the air intake model with dimensions is shown in figure 1(a). The selection of the tube inlet is primarily governed by the position of the normal/ $\lambda$ -shock near the throat of the air intake. Beneath this  $\lambda$ -shock, the pressure rises significantly, leading to a strong interaction region dominated by SWBLI. In their study, Das et al.[1] proposed the use of bleed to extract the low-energy fluid from this region to mitigate the adverse effects; however, this approach resulted in a reduction of the overall mass flow rate. Building on this concept, the idea emerged to re-inject the extracted flow back into the intake, rather than discarding it. Accordingly, the size of the tube inlet was determined based on the bleed size used by Das et al.[1]. For ease of meshing and geometric simplicity, a rectangular cross-section was chosen for the tube. Furthermore, the tube exit was positioned at different locations, particularly at the junctions of the shoulder and diffuser, diffuser-to-diffuser, and diffuser-to-isolator. To investigate the impact of area expansion, Case 4 was specifically designed.

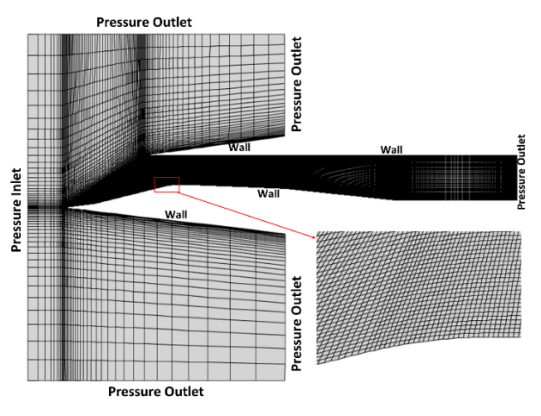


Figure 2. Mesh along with opted boundary condition (grid 2)

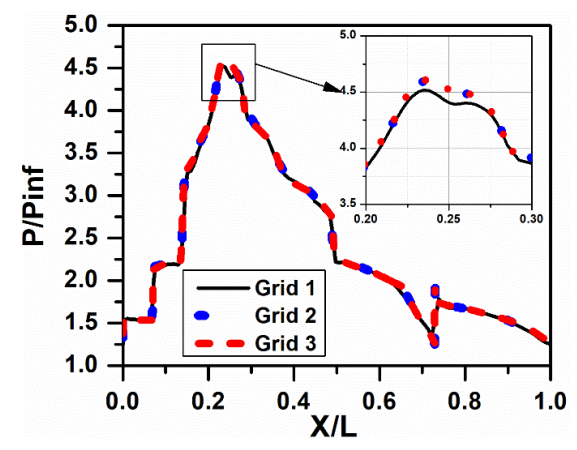


Figure 3. Static pressure distribution over ramp surface

Four different configurations, referred to as Case 1 through Case 4, are illustrated in Figures 1b to 1e. Each configuration varies based on the exit location, while the starting point remains the same for all cases. The rectangular tube used in first three case has a uniform cross-sectional dimension of 2 mm. The tube is

designed such that its lower surface aligns with the isolator surface of the air intake. In Case 1, the tube exit is positioned at the beginning of the first diffuser, forming a 'C'-shaped path. In Case 2, the exit is located at the end of the first diffuser, maintaining the same 'C'-shaped geometry. In Case 3, the exit is placed at the junction between the second diffuser and the start of the isolator section, forming an 'L'-shaped configuration. Case 4 features an increased area compared to Case 3 and extends to cover the entire region beneath the ramp surface of the air intake, as depicted in figure 1e.

#### 3. METHODOLOGY

Commercially available software Ansys 2019 was used for modeling and simulations of all the cases. The simulations involved in this study has been performed by using Ansys fluent at NIT Kurukshetra, Haryana, India. Mass, momentum, and energy conservation were computed using the Reynolds-averaged Navier-Stokes (RANS) equations. To capture the turbulent flow, the kω SST turbulence model was chosen, as it is widely used in aerospace applications, employed in the authors' previous study [31], and recommended by other researchers [32]. A structured hexahedral grid was employed in this study, with the near-wall flow physics of the air intake resolved using a minimum wall-normal grid spacing of approximately 0.15 mm, corresponding to a y $\square$  value of about 25[1]. Near the junction point, a grid clustering option was chosen in a span-wise direction. A sample of the grid along with the boundary conditions and the extended computational domain are shown in Figure 2. At the air intake, a pressure inlet condition was imposed. Every flow out segment had a pressure outlet condition, and the air intake wall surfaces had a wall boundary condition. All simulations were conducted at a design Mach number of 2.2. The freestream total pressure and temperature were fixed at 308,145 Pa and 300 K, respectively.

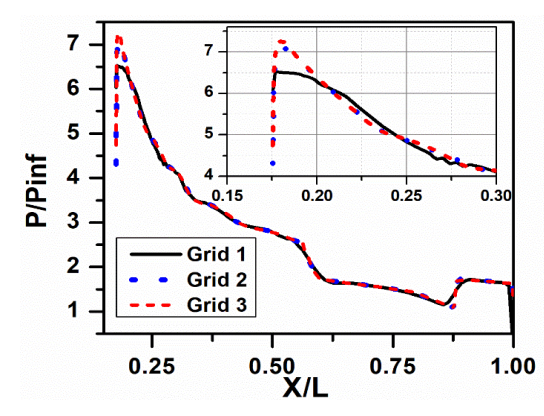


Figure 4. Static pressure distribution over cowl surface

Static gauge pressures were then computed using isentropic relations. The working fluid selected is air, based on the assumptions of the ideal gas law. Sutherland's law was used to model the viscosity. A free stream turbulent intensity of 0.5% was specified at the inlet [1]. Throughout the simulations, continuity, energy residuals and area weighted average Mach number over the ramp surface were monitored, with the convergence criterion set at a residual value of approximately  $10 \Box^3$ .

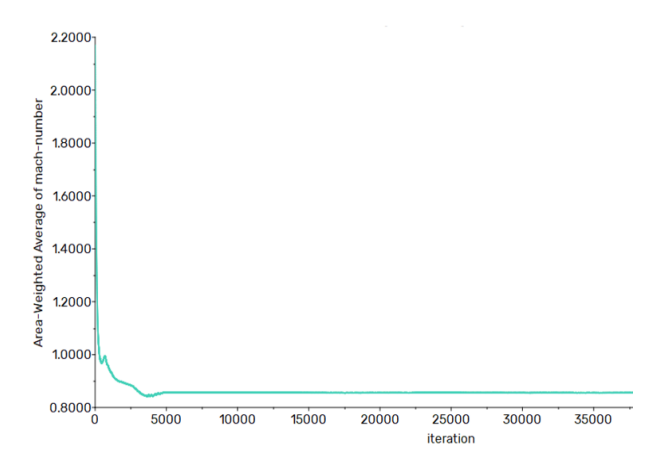


Figure 5. Area weighted average of Mach number Vs No of iterations over the ramp surface of the air intake

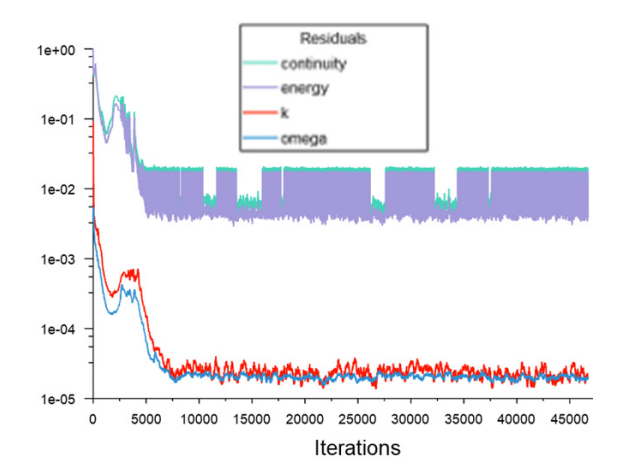


Figure 6. Residuals showing the convergence history.

Mach number plot and residual plot vs number of iterations are shown in figure 5 and 6 respectively. To ensure that the outcomes were independent of the mesh resolutions, a two-step grid independence test was carried out in the present study, following the methodology adopted in author(s) earlier work [31] and in line with the recommendations of Das et al. [1]. In the first step, the wall-normal spacing was examined by considering different first-cell heights. A first-cell height of approximately 0.15 mm was selected based on previous validation and suitability for capturing the near-wall behavior. In the second step, three levels of grid (Grid 1: 8.400 elements, Grid 2: 83.200 elements and Grid 3: 112,400 elements) refinement were generated and compared. The static pressure distribution over the ramp and cowl surfaces is illustrated in figures 3 and 4, respectively, while the density contours for all three grid systems are shown in figure 7. The simulations successfully captured key flow features, including the shock structure, flow spillage near the cowl tip, and flow separation along the ramp surface near the throat section inside the air intake. Additionally. Mach numbers at three different locations in the vicinity of the lambda shock were compared across the grid systems. It was observed that the Mach number values obtained from grid 2 and grid 3 closely matched, indicating a high level of consistency between these two grids. In contrast, grid 1 showed a slight deviation in Mach number values, which is evident in the zoomed-in

views of the pressure distributions over the ramp and cowl surfaces. Among these, Grid 2 was finalized for the present computations, as it provided a good balance between accuracy and computational cost. To further confirm the adequacy of the selected grid, an additional finer mesh with a first-cell height of the order of 0.00015 mm (corresponding to  $y \square < 1$ ) was also studied. The results of this finer grid were compared against both the experimental data [1] and the present compu-tation at  $y \square \approx 25$ . The results are compared in Figure 8, the pressure distributions predicted by the selected grid (Grid 2) are in close agreement with both experimental measurements and the finer grid results. These compa-risons demonstrate that the employed grid is sufficiently fine to capture the essential flow physics inside the air intake, ensuring grid-independent results for the present study.

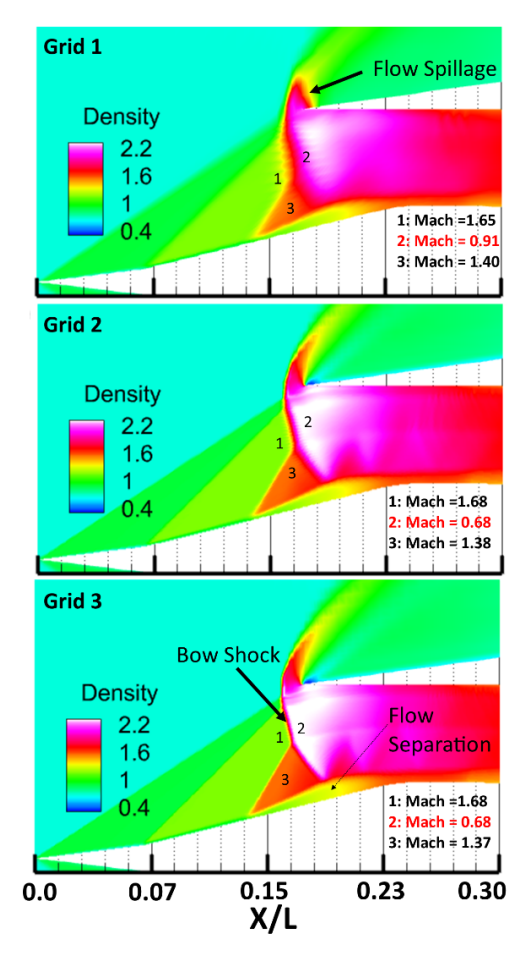


Figure 7. Density contour at various grid

### 4. VALIDATION STUDY OF ADOPTED METHODOLOGY

To verify the accuracy of the computed results, validation is crucial. So, a validation test was performed to ensure that the numerical approach was accurate. The computational results of ramp pressure distribution were compared with that of experimental results from the findings from Das and Prasad's study[1]. which is shown in figure-8. Overall, there is good agreement between the computational results and the reference experiment[1] results. A closer inspection, however, reveals a modest discrepancy in between X/L of 0.2 to

0.3 in figure 8. This variation is plausibly attributed to the differing dimensional assumptions: the present analysis is strictly two-dimensional, whereas the reference solution was generated from a fully three-dimensional model. Figure 8 can confirmed that the 2-d grid resolution and numerical scheme are sufficient for capturing the dominant physics of the intake flow field for preliminary design purposes.

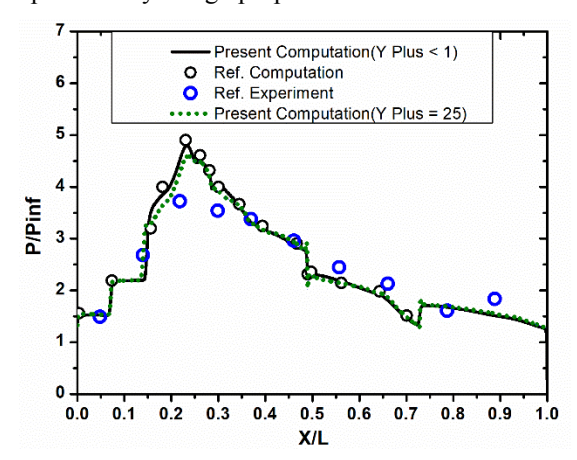


Figure 8. Ramp pressure distribution (validation test)

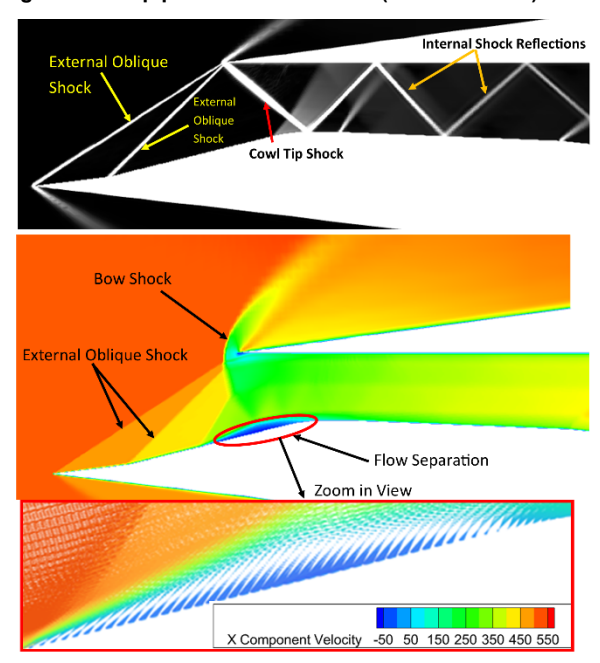


Figure 9. (a)Top: Density Gradient contour (Inviscid) (b) Bottom: X velocity (m/s) contour (Viscous) and x velocity vector contour for zoom in view

#### 5. RESULTS AND DISCUSSION

To gain insight into the unstart phenomenon in a mixed-compression supersonic intake, the baseline configuration was first analyzed both with and without viscous effects. Figure 9a presents the density gradient contour for the inviscid case, where a well-defined system of shock waves originates from the first and second ramp, which further combines with the cowl lip shock and undergoes multiple reflections inside the duct. Such a pattern is indicative of a started intake, with the supersonic core flow preserved. When viscous effects were incorporated using the  $k-\omega$  SST turbulence model, however, the intake exhibited a markedly

different response. As illustrated in Figure 9b, the xvelocity contour highlight signatures of unstart, wherein the internal shock system loses its stability and is expelled upstream of the duct. Detailed examination of the zoomed velocity-vector contours in the separation region further confirms this behavior: flow reversal is clearly visible, with local velocities reaching as low as – 50 m/s. This recirculation zone indicates a significant separation bubble forming near the throat region, consistent with mechanisms widely described in the literature as a "soft unstart" [13]. In such cases, the cowl -induced shock interacts unfavorably with the growing boundary layer, leading to pronounced thickening and a reduction in the effective throat area ratio. The corresponding decrease in contraction ratio disrupts the internal shock structure, causing it to be expelled from the duct near the cowl lip. This process collapses the supersonic core into subsonic flow, culminating in full intake unstart.

To address the issue of intake-unstart, the subsequent section explores the application of a pressure feedback technique across four different cases. The results from these configurations are then compared with the baseline model to evaluate their effectiveness in mitigating unstart behaviour and improving intake stability.

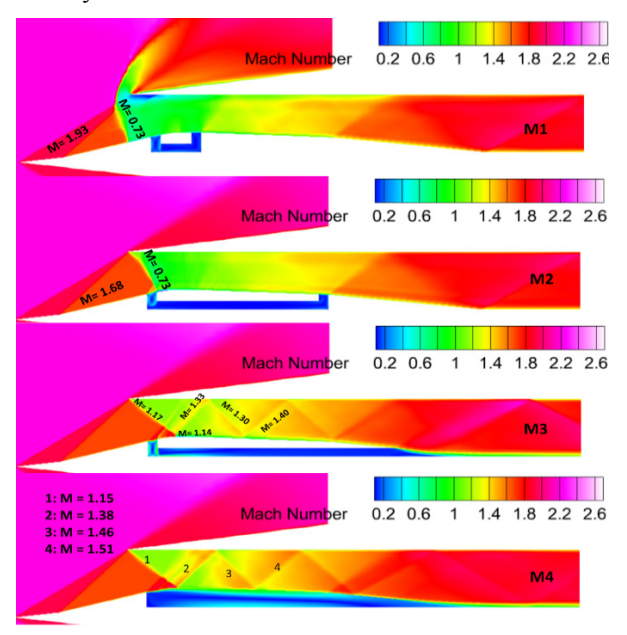


Figure 10. Mach No contour for all the modified cases.

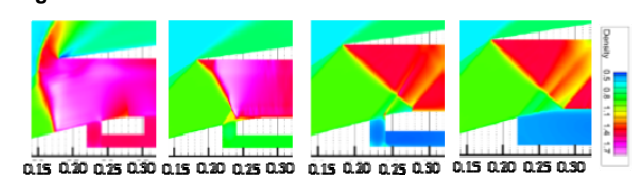


Figure 11. Density contour (zoom in view near the throat) for all the modified cases. (Starting from left)

Four distinct cases of the Pressure Feedback Technique, referred to as M1, M2, M3, and M4, were investigated computationally at a design Mach number of 2.2 with a cowl deflection angle of zero degrees. Figure 10 illustrates the Mach number contour comparisons within the air intake for each case. Oblique shock

waves were generated from the first and second ramps of the intake, which, under ideal conditions, should impinge directly on the cowl lip. However, in cases M1 and M2, a bow shock wave was still present, indicating a shift in the shock foot location. Although the postbow-shock Mach number remains consistent between cases M1 and M2, a significant difference is observed in the flow spillage characteristics. In case M1, flow spillage occurs near the cowl lip, whereas in case M2, this spillage is eliminated. Despite the improvement in flow control, the absence of further internal shock reflections suggests that the intake remains in a nonstarted condition. In contrast, cases M3 and M4 display complete shock reflections within the intake duct, indicating that the intake has achieved a fully started condition. Based on this comparison, it can be inferred that the intake in case M2 is in a transitional or nearstarted state. Additional insights are provided by the zoomed-in density contour presented in Figure 11. In case M2, the bow shock exhibits a dual lambda structure, with one leg located near the cowl side and the other near the ramp side. The variation in the location of the cowl originated shock foot along the ramp surface is also evident. For case M1, the shock foot lies between X = 0.15 mm and 0.20 mm from the origin (ramp tip), whereas in case M2, it shifts downstream to approximately X = 0.25 mm. In cases M3 and M4, the shock foot moves further downstream, reaching close to X = 0.30 mm.

Figures 12 and 13 present the static pressure distributions along the ramp and cowl surfaces of the air intake for both the baseline configuration and the modified cases M1 through M4. The x-axis is non-dimensionalized with respect to the ramp length (X/L), allowing for a consistent comparison across configurations. Along the first ramp segment, from the leading edge up to approximately X/L = 0.05, the static pressure remains nearly constant for all configurations, indicating undisturbed supersonic flow prior to the first compression corner. A noticeable pressure rise is observed at the start of the second ramp (around X/L =0.05), which corresponds to the formation of an oblique shock generated by the change in ramp angle. For the baseline, as well as for cases M2, M3, and M4, the pressure remains relatively uniform across the second ramp surface until about X/L = 0.15, reflecting a stable attached shock with minimal disruption. However, case M1 shows a significantly higher pressure rise in this region compared to the baseline, suggesting that the bow shock developed downstream in M1 is stronger than that in the unmodified intake.

Around X/L = 0.15-0.2, an additional pressure rise is recorded, which corresponds to the interaction of the flow with the bow shock near the cowl lip. This effect is most pronounced in the baseline and M1 cases, both of which exhibit noticeable flow spillage at the cowl lip. The magnitude of the pressure peak in M1 further confirms the increased strength of the bow shock in this configuration. In contrast, the pressure distributions in cases M2, M3, and M4 remain smoother across this region, with case M2 showing a slight rise in pressure near the throat, an indication of mild flow blockage, while cases M3 and M4 exhibit a small pressure drop

due to local expansion effects. This localized expansion helps in controlling flow separation and supports the intake in M3 and M4 remains in a started condition, even under off-design conditions[2]. Further downstream, beyond X/L=0.20, the pressure distributions reveal oscillations characterized by alternating rises and falls resulting from multiple shock reflections and boundary layer interactions within the internal duct. These fluctuations indicate the ongoing compression and adjustment of the flow as it progresses through the intake system.

The pressure behavior over the cowl surface, as shown in Figure 13, supports these findings. A sharp pressure peak is seen near X/L = 0.19 for both the baseline and M1 configurations, marking the location where the bow shock impinges on the cowl lip and where external spillage originates. In contrast, this peak is significantly reduced in M2 and nearly absent in M3 and M4, implying that spillage is progressively minimized with each successive modification. The downstream pressure levels on the cowl for M3 and M4 are more uniform, consistent with fully started conditions where internal shock structures are confined within the duct and no longer interact with the external flow.

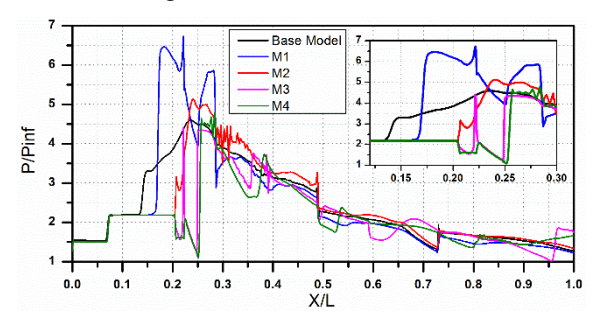


Figure 12. Static pressure distribution over Ramp surface for all cases

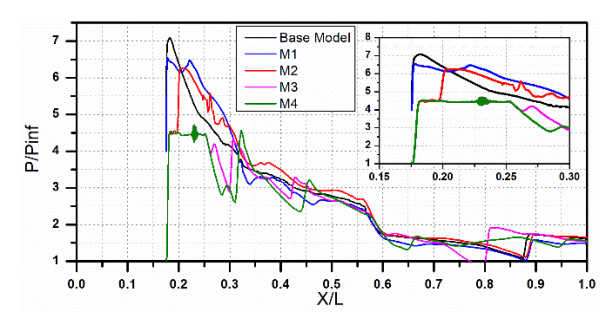


Figure 13. Static pressure distribution over Cowl surface for all cases

Figure 14 illustrates the contours of the x-component velocity for four pressure-feedback configurations and highlights the role of the pressure difference between Location 1 and Location 2 in determining whether the intake remains un-started (M1 and M2) or transitions to a started state (M3 and M4). The two locations are connected through the pressure-feedback tube, and for each case, the area-weighted average pressure is evaluated at both points. This enables direct comparison of pressure values and provides insight into the effective pressure gradient, which dictates the direction of flow through the tube. In Case M1, the pressure ratio at Location 1 is 6.01, while at Location 2 it is 5.80, resulting in only a small pressure difference of 3.3%.

Although a higher static pressure exists near the suction port, the reversed flow at Location 1 (about -100 m/s) fills the entrance of the PFT tube, restricting mass extraction. A reduction in throat separation over the ramp surface is observed compared with the base model; however, the intake remains in the un-started state.

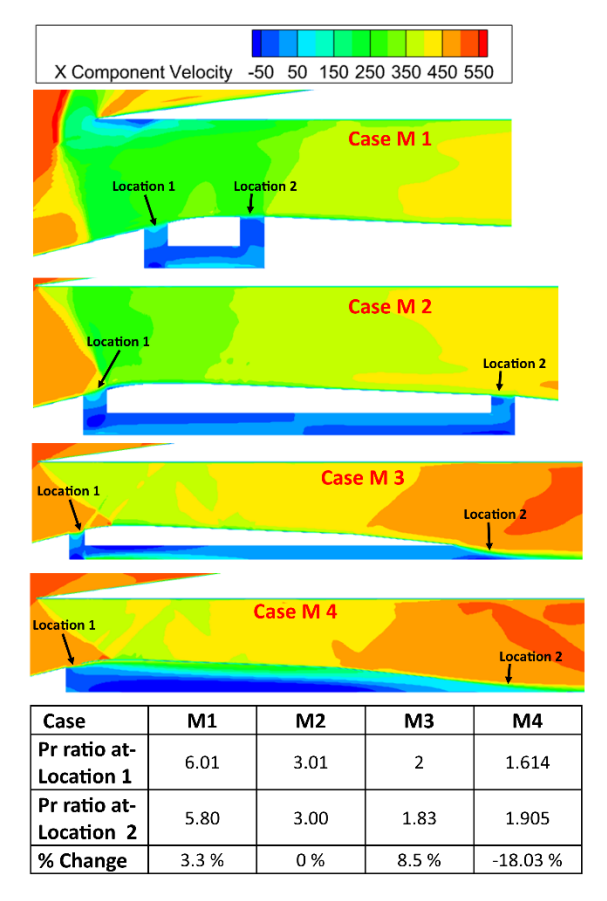


Figure 14. X component velocity contour of the Pressure Feedback Technique tube region.

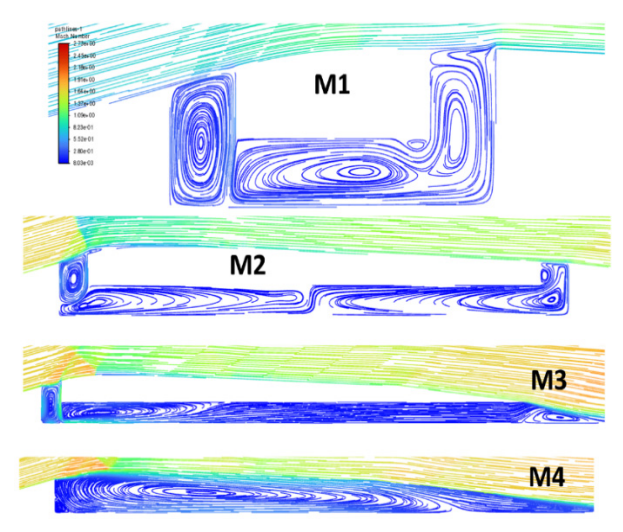


Figure 15. Streamline Pattern inside the Pressure Feedback Technique tubes. Direction of flow is from left to right.

A similar condition is observed in Case M2, where the pressure ratios at Location 1 and 2 are nearly equal (3.01 vs. 3.00, 0% difference), again producing negligible mass transfer through the tube. The streamline contours (Figure 15) confirm recirculation and blockage inside the tube for both M1 and M2. However, since the

tube cross-sectional area is increased in Case M2, more room is available for the retarded flow. Consequently, the bow shock is transformed into an oblique shock, indicating behaviour that is on the verge of intake starting. In Case M3, a more effective pressure difference is established: the pressure ratio at Location 1 is 2.0, while at Location 2 it is 1.83, corresponding to a larger gradient of 8.5%. This pressure drop across the tube enables significant flow from the high-pressure separation pocket at Location 1 toward Location 2. The separation bubble at the suction port, though reduced compared with the base model, still introduces blockage. Nevertheless, some mass transfer occurs, which helps establish a favourable pressure gradient within the duct and drives the intake to a fully started condition. Finally, in Case M4, the pressure ratio at Location 1 reduces further to 1.614, while at Location 2 it increases slightly to 1.905, resulting in a negative pressure difference (-18.03%). In this case, Location 2 actually has a higher pressure than Location 1, which reverses the intended suction effect of the PFT and disrupts flow transfer. As a result, the PFT principle becomes ineffective, and flow attachment is adversely affected, even though the intake exhibits behaviour closer to a started state compared to M1 and M2, just because an increased area of the tube.

#### 6. PERFORMANCE PARAMETRS:

The distribution of the computed total pressure at the exit of the diffuser for all modified cases is illustrated in Figure 16. An overall improvement in total pressure is observed across all configurations when compared to the baseline. However, in case M1, the improvement is minimal and can be considered negligible. In contrast, cases M2, M3, and M4 exhibit significant enhancements in total pressure at the isolator exit, indicating more effective internal flow management and reduced total pressure losses.

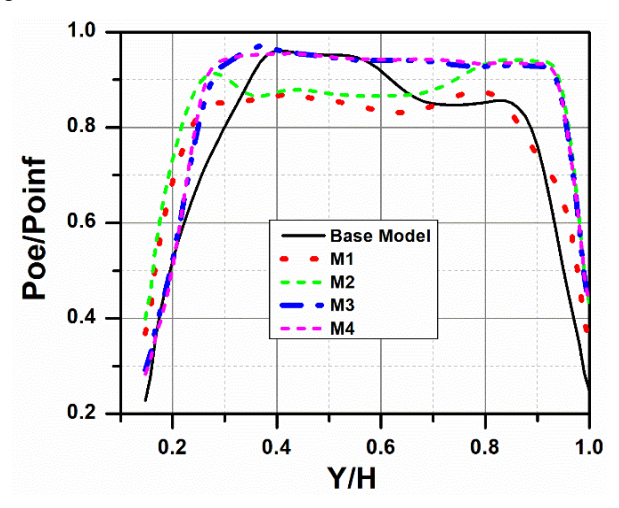


Figure 16. Total pressure distribution at the exit of the air intake

To quantitatively assess the performance of the air intake, two key performance metrics were evaluated: total pressure recovery (TPR) and flow distortion (FD). Total pressure recovery is defined as the ratio of the area-weighted total pressure at the isolator exit  $(P \square \square)$ 

to the free-stream total pressure  $(P \square \infty)$ . Flow distortion, on the other hand, is calculated as the ratio of the difference between the maximum and minimum total pressures at the exit to the area-weighted average total pressure.

These performance parameters were computed following the formulations proposed by Javed et al.[33]. The summary of TPR and FD values for the base model and the modified configurations is presented in Table 1. The Base Model yields a TPR of 0.73 and a corresponding FD of 0.73, serving as the reference for evaluating the modifications. In case M1, a marginal increase in TPR is observed (0.74), corresponding to a 1.36% improvement. However, a notable enhancement is seen in the FD, which drops significantly to 0.52 representing a 28.76% reduction in distortion. This implies that although the total pressure recovery remains nearly unchanged, M1 effectively suppresses some of the flow irregularities. In case M2, the performance improvement is more pronounced, with TPR increasing to 0.81, signifying a 10.95% enhancement over the base model. The FD is also significantly improved, dropping to 0.54 (a 26.02% reduction). This suggests that the intake is transitioning toward a fully started condition with better flow uniformity and reduced pressure losses. Cases M3 and M4 also show strong TPR value of 0.80 corresponding to 9.58 % increase relative to the base case. However, unlike M2, the flow distortion values for M3 and M4 (0.67 and 0.66) are slightly higher than that of M2 but still significantly lower than the baseline. Their FD improvements are 8.21% and 9.58%, respectively. These results indicate that while M2 offers the best balance between pressure recovery and flow uniformity, M3 and M4 still ensure high pressure recovery with moderate control over distortion. M1, despite offering minimal pressure recovery, demonstrates a major reduction in flow distortion. Overall, the Pressure Feedback Technique (PFT) is proven effective in enhancing the performance of the air intake system, especially in cases M2, M3, and M4.

Table 1. Summary of Pressure recovery and flow distortion

	TPR	% TPR	FD	%FD
Base	0.73		0.73	
Model				
M1	0.74	1.36	0.52	-28.76
M2	0.81	10.95	0.54	-26.02
M3	0.80	9.58	0.67	-8.21
M4	0.80	9.58	0.66	-9.58

#### 7. EFFECT OF MACH NUMBER

The performance of the best configuration (Case M3) was analyzed at Mach numbers 2.0, 2.2, and 2.5, and the results are presented through Mach contours (Figure 17), pressure distributions (Figure 18 and 19), and performance indices (Table 2). At Mach 2.0, the intake still exhibits unstart behavior despite the use of the pressure feedback tube, with a bow shock forming at the throat causing spillage at the cowl lip; no effective shock reflections occur inside the air intake, and the static pressure distribution shows abnormally high

peaks, almost double compared to the other cases. In contrast, at the design Mach number of 2.2, the intake operates in a started condition, where the oblique shocks from the ramps interact properly with the cowl lip and stabilize inside the isolator, leading to smoother pressure change along the ramp, and the most uniform exit total pressure distribution. At Mach 2.5, however, the oblique shocks generated by the ramps fail to meet the shock-on-lip condition which introduces additional distortion. The performance indices summarized in Table 2 further reinforce these trends: Mach 2.2 achieves the highest total pressure ratio (0.80) and distortion (0.67), while Mach 2.0 shows a 3.75% drop in TPR and unstart-related penalties, and Mach 2.5 suffers the largest loss with an 8.75% reduction in TPR and a 7.46% increase in distortion. Overall, it can be concluded that Case M3 with pressure feedback performs optimally at Mach 2.2, while both lower and higher Mach numbers degrade intake performance due to unstart and internal shock on lip condition respectively.

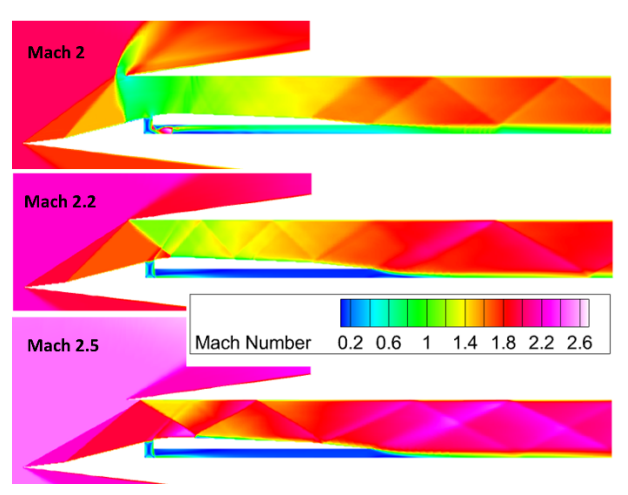


Figure 17: Mach contour for case M3

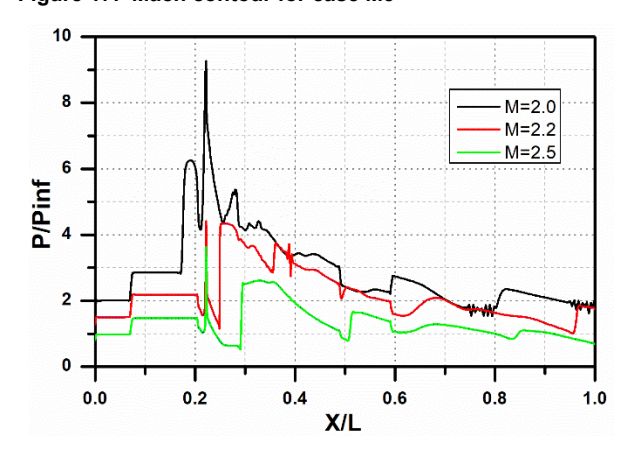


Figure 18. Static pressure distribution over the ramp surface for case M3.

Table 2. Performance parameters with reference to Case M3

Case M3	TPR	% TPR	FD	% FD
Mach 2.2	0.8	-	0.67	
Mach 2	0.77	-3.75	0.64	-4.47
Mach 2.5	0.73	-8.75	0.72	7.46

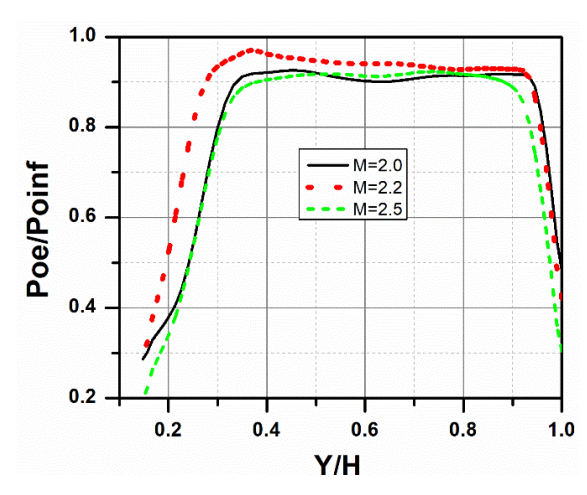


Figure 19. Total pressure distribution at the exit of the air intake for case M3.

#### 8. CONCLUSION

The computational investigation of four modified air intake configurations designated as M1, M2, M3, and M4 using the pressure feedback technique (PFT) at a design Mach number of 2.2 with zero-degree cowl deflection has provided valuable insights into the flow control and performance enhancement potential of such modifications. Initial analysis of Mach number contours revealed the presence of oblique shocks generated from the first and second ramps of the air intake. In cases M1 and M2, despite the expectation that these shocks would impinge directly on the cowl lip, a bow shock persisted, although with altered shock foot positions. The flow spillage, which remained visible near the cowl lip in M1, was significantly reduced in M2. Further comparisons with M3 and M4 demonstrated a complete shock reflection inside the intake duct, indicating successful intake self-start conditions. Static pressure distributions along the ramp and cowl surfaces also supported these findings. While M1 exhibited a sharp pressure rise, indicating a stronger bow shock than the base model, M2 maintained a more stable pressure trend with a controlled rise near the throat, suggesting a movement toward the started condition. M3 and M4, on the other hand, displayed a pressure drop indicative of local flow expansion and improved shock control, enabling better suppression of flow separation even under off-design conditions. Further insights were drawn from the analysis of x-direction velocity contours and streamline patterns. In M1 and M2, separation bubbles with negative velocities around -100 m/s appeared near the suction point of the PFT tube, effectively blocking mass flow extraction and maintaining the unstart condition. However, in M3 and M4, this blockage was alleviated, allowing continuous mass transfer from the separation region to downstream low-pressure zones.

Quantitative assessment through performance parameters, total pressure recovery (TPR) and flow distortion (FD), further validated these findings. Case M1 showed negligible TPR improvement (1.36%) but a substantial reduction in FD (28.76%), suggesting partial regulation of flow unsteadiness. Case M2 exhibited the highest TPR (a 10.95% increase) and a significant FD reduction (26.02%), demonstrating an effective tran-

sition toward a near-started condition with both high-pressure recovery and flow uniformity. M3 and M4 followed closely with TPR improvements of 9.58%, and moderate FD reductions of 8.21% and 9.58% respectively, indicating reliable performance under started conditions with slightly less distortion control compared to M2. Mach number effect for Case M3 was also investigated, and the results indicate that the intake performs best at Mach 2.2 with stable shock interactions, maximum pressure recovery, and minimum distortion. At Mach 2.0, unstart caused by the bow shock leads to significant performance degradation, whereas at Mach 2.5, failure to satisfy the shock-on-lip condition results in internal shock reflections and increased distortion.

In conclusion, the pressure feedback technique proves to be a robust passive flow control method for enhancing the startability and performance of supersonic air intakes. Among the configurations investigated, M2 strikes the most optimal balance between pressure recovery and flow distortion, making it a strong candidate for practical application but air intake is in unstart condition. M3 and M4 offer excellent performance under started flow conditions with consistent pressure recovery and manageable distortion. Meanwhile, M1, though not as effective in total pressure enhancement, demonstrates that even minimal geometric modifications can significantly suppress flow irregularities. These findings underscore the potential of PFTbased design strategies to improve air intake operability, especially in regimes close to critical start conditions

#### **ACKNOWLEDGMENTS**

Authors are thankful to NIT Kurukshetra, and Amity University Uttar Pradesh for providing their support in conducting the research work.

#### **REFERENCES**

- [1] S. Das, J. K. Prasad, "Starting characteristics of a rectangular supersonic air-intake with cowl deflection," *Aeronaut. J.*, vol. 114, no. 1153, pp. 177–189, 2010, doi: 10.1017/S0001924000003626.
- [2] J. Sinha, S. Singh, O. Prakash, D. Panchal, "Passive Flow Modification Over the Supersonic and the Hypersonic Air-Intake System Using Bleed," *FME Trans.*, vol. 51, no. 3, pp. 329–337, 2023, doi: 10.5937/fme2303329S.
- [3] M. R. Soltani, A. Daliri, J. Sepahi Younsi, "Effects of shock wave/boundary-layer interaction on performance and stability of a mixed-compression inlet," *Sci. Iran.*, vol. 23, no. 4, pp. 1811–1825, 2016, doi: 10.24200/sci.2016.3928.
- [4] D.S. Dolling, "Fifty Years of Shock-Wave/Boundary-Layer Interaction Research: What Next?," *AIAA J.*, vol. 39, no. 8, pp. 1517–1531, 2001, doi: 10.2514/3.14896.
- [5] F. Gnani, H. Zare-Behtash, C. White, K. Kontis, "Numerical investigation on three-dimensional shock train structures in rectangular isolators," *Eur. J. Mech. B/Fluids*, vol. 72, no. August, pp. 586–593, 2018, doi: 10.1016/j.euromechflu.2018.07. 018.

- [6] N. Titchener, H. Babinsky, "Microvortex generators applied to flowfield containing a normal shock wave and diffuser," *AIAA J.*, vol. 49, no. 5, pp. 1046–1056, 2011, doi: 10.2514/1.J050760.
- [7] P. Vivek, S. Mittal, "Buzz Instability in a Mixed-Compression Air Intake," *J. Propuls. Power*, vol. 25, no. 3, pp. 819–822, 2009, doi: 10.2514/1.39751.
- [8] A. L. Philippou, P. K. Zachos, D. G. MacManus, "Aerodynamic Instabilities in High-Speed Air Intakes and Their Role in Propulsion System Integration," *Aerospace*, vol. 11, no. 1, 2024, doi: 10.3390/aerospace11010075.
- [9] N. K. Gahlot, N. K. Singh, "Parametric Study on Influence of an Array of Air Jets on the Performance of Supersonic Air Intake by Varying the Jet Injection and Back Pressure," *J. Aerosp. Eng.*, vol. 34, no. 6, p. 04021086, 2021, doi: 10.1061/(asce) as.1943-5525.0001337.
- [10] A. K. Flock, A. Gülhan, "Modified Kantrowitz starting criteria for mixed compression supersonic intakes," *AIAA J.*, vol. 57, no. 5, pp. 2011–2016, 2019, doi: 10.2514/1.J057283.
- [11] S. Emami, C. A. Trexler, A. H. Auslender, J. P. Weidner, "Experimental investigation of inlet-combustor isolators for a dual-mode scramjet at a Mach number of 4," NASA Tech. Pap. 3502, no. May, 1995.
- [12] S. Janarthanam and V. Babu, "Numerical simulations of the flow through the inlet and isolator of a Mach 4 dual mode scramjet," *Aeronaut. J.*, vol. 116, no. 1182, pp. 833–846, 2012, doi: 10.1017/s0001924000007302.
- [13] S. Das, J.K. Prasad, "Unstart suppression and performance analysis of supersonic air-intake adopting bleed and cowl bending," *J. Inst. Eng. Aerosp. Eng. J.*, vol. 91, no. MAY, pp. 27–35, 2010, doi: 10.4028/www.scientific.net/AMR.864-867.347.
- [14] M.C. Neale, P.S. Lamb, "Tests with a Variable Ramp Intake Having Corn bined External/Internal Compression, and a Design Mach Number of 2.2," *Aeronaut. Res. Counc.*, no. CP-805, pp. 1–35, 1962.
- [15] J. Sinha, S. Singh, O. Prakash, D. Panchal, "Analysis of Supersonic Intake Design for Multi-Row Disk Intake Device Under Varying Mach Numbers and Angle of Attacks," *FME Trans.*, vol. 53, pp. 38–50, 2025, doi: 10.5937/fme2501038S.
- [16] D. Mahapatra, G. Jagadeesh, "Studies on unsteady shock interactions near a generic scramjet inlet," *AIAA J.*, vol. 47, no. 9, pp. 2223–2231, 2009, doi: 10.2514/1.41954.
- [17] S. Vaisakh, T. M. Muruganandam, "Control of Boundary Layer Separation in Supersonic Flow Using Injection Through Microramps," Springer Int. Publ. AG 2017 G. Ben-Dor al. (eds.), 30th Int. Symp. Shock Waves 2, doi: 10.1007/978-3-319-46213-4.
- [18] E. Erdem, K. Kontis, E. Johnstone, N.P. Murray, J. Steelant, "Experiments on transitional shock wave Boundary layer interactions at Mach 5," *Exp.*

- Fluids, vol. 54, no. 10, 2013, doi: 10.1007/s00348-013-1598-z.
- [19] C. Zhang, Y. Luo, H. Liang, S. Guo, H. Yang, "Experimental and Numerical Study on Incident Shock Wave/Boundary Layer Interaction Control," *Actuators*, vol. 11, no. 6, 2022, doi: 10.3390/act 11060148.
- [20] M.R. Soltani, M. Farahani, J. Sepahi Younsi, "Performance study of a supersonic inlet in the presence of a heat source," *Sci. Iran.*, vol. 18, no. 3 B, pp. 375–382, 2011, doi: 10.1016/j.scient.2011.05.027.
- [21] T. Jana, M. Kaushik, "Survey of control techniques to alleviate repercussions of shock-wave and boundary-layer interactions," *Adv. Aerodyn.*, vol. 4, no. 1, 2022, doi: 10.1186/s42774-022-00119-9.
- [22] H. Babinsky, N. Makinson, C. Morgan, "Micro-Vortex Generator Flow Control for Supersonic Engine Inlets," 45th AIAA Aerosp. Sci. Meet. Exhib., no. January, p. 2007, 2007, doi: 10.2514/6.2007-521.
- [23] J. Slater, "Improvements in Modeling 90-degree Bleed Holes for Supersonic Inlets," *J. Propuls. Power*, vol. 28, no. 4, pp. 773–781, 2012, doi: 10.2514/1.B34333.
- [24] N. Hildebrand, A. Dwivedi, J. W. Nichols, M. R. Jovanović, G. V. Candler, "Simulation and stability analysis of oblique shock-wave/boundary-layer interactions at Mach 5.92," *Phys. Rev. Fluids*, vol. 3, no. 1, 2018, doi: 10.1103/PhysRevFluids.3. 013906.
- [25] J. Zhai, C.A. Zhang, F.M. Wang, W.W. Zhang, "Control of shock-wave/boundary-layer interaction using a backward-facing step," *Aerosp. Sci. Technol.*, vol. 126, p. 107665, 2022, doi: 10.1016/j.ast.2022.107665.
- [26] N. K. Gahlot, N. K. Singh, "Flow Field Study of Mixed Compression Supersonic Air Intake with Cowl Ventilation," *J. Appl. Fluid Mech.*, vol. 13, no. 6, pp. 1795–1805, 2020, doi: 10.36884/jafm. 13.06.31428.
- [27] S. Ogura et al., "Experimental study of high-speed air intake performance by side clearance," *Aerosp. Sci. Technol.*, vol. 123, p. 107439, 2022, doi: 10.1016/j.ast.2022.107439.
- [28] S. Desai, V. Kulkarni, H. Gadgil, "Separation mitigation using pressure feedback technique for hypersonic shock wave boundary layer interaction," *Proc. Inst. Mech. Eng. Part G J. Aerosp. Eng.*, vol. 233, no. 10, pp. 3519–3533, 2019, doi: 10. 1177/0954410018802959.
- [29] A.A. Kane, R.K. Peetala, V. Kulkarni, "Investi-gation of pressure feedback technique to control ramp based SWBLI," *Acta Astronaut.*, vol. 201, no. January, pp. 482–495, 2022, doi: 10.1016/j.acta astro.2022.09.057.
- [30] X. yu Zhong, W. Huang, L. Yan, H. Wu, Z. bo Du, "Investigation on the adaptive control of shock wave/turbulent boundary layer interaction based on the secondary circulation jets," *Acta Astronaut.*,

vol. 198, no. June, pp. 233–250, 2022, doi: 10.1016/j.actaastro.2022.06.016.

- [31] N. K. and S. N. Gahlot, "Effect of air jet with injection pressure on the performance of mixed compression air intake," *Proc IMechE Part G J Aerosp. Eng.*, pp. 1–13, 2020, doi: 10.1177/0954410020966507.
- [32] V.R. Petha Sethuraman, H. D. Kim, "Characteristics of Shock Train Flow in Divergent Channels," *J. Appl. Fluid Mech.*, vol. 13, no. 4, pp. 353–364, 2020, doi: 10.1007/978-981-15-1892-8\_28.
- [33] M. R. Soltani, J. Sepahi Younsi, V. Farajpoor Khanaposhtani, "Numerical investigation of the unstart suppression in a supersonic air intake," *Iran. J. Sci. Technol. Trans. Mech. Eng.*, vol. 39, no. M2, pp. 413–426, 2015.

#### **NOMENCLATURE**

Н	Height of Air intake, mm
L	Length of Air intake, mm
P	Static pressure, Pascal
Po	Total pressure, pascal
M	Mach Number
X	Length in X direction
Y	Height in Y direction

#### Abbreviations

X/L

Y/H

1100.07.00.00		
Reynolds Averaged Navier Stokes		
Pressure Feedback Technique		
k–ω Shear Stress Transport		
Total Pressure Recovery (ratio of total		
average pressure at Air Intake's exit to that		
of free-stream total pressure.)		
Flow Distortion (ratio of difference in		
maximum and minimum total pressure to that		
of total average pressure at Air Intake's exit.)		
Shock wave boundary layer interaction		
Computational Fluid Dynamics		
Ratio of static pressure at a point to that of		
free-stream static pressure		
Ratio of total pressure at Air Intake's exit to		
that of free-stream total pressure.		

of total length of Air-Intake.

Ratio of length from origin at a point to that

Ratio of height from bottom at a plane to that

of total height of Air-Intake

#### Subscripts

e Exit of Air Intake inf Free stream condition

## ТЕХНИКА ПОВРАТНЕ СПРЕГЕ ПРИТИСКА ЗА ПОБОЉШАЊЕ ПЕРФОРМАНСИ НАДЗВУЧНОГ УСИСНИКА ВАЗДУХА ПРИ МАХОВОМ БРОЈУ ОД 2.2

#### С. Курана, Н.К. Галот, Н.К. Синг

Ова студија представља свеобухватно рачунарско истраживање надзвучног усисника мешовитог компресионог ваздуха модификованог коришћењем технике повратне спреге притиска (PFT) ради побољшања стартовања и перформанси при пројектованом Маховом броју од 2,2 са отклоном поклопца од нула степени. Четири различите конфигурације, означене као М1, М2, М3 и М4, анализиране су и упоређене са основним моделом. Утицај РFТ-а на структуре удара, раздвајање тока и расподелу притиска унутар усиса систематски је процењен коришћењем контура Маховог броја и брзине, графикона густине и визуелизација линија струје. RANS једначине су решене коришћењем k-omega SST модела турбуленције у софтверском пакету Ansys CFD. Резултати су показали да су случајеви М3 и М4 постигли потпуно стартно стање, карактерисано потпуно развијеним рефлексијама удара и побољшаним понашањем унутрашњег тока. Случај М2 је показао скоро стартно стање са контролисаним понашањем удара прамца и минималним преливањем тока, док је М1 остао у непокретном стању, али је показао смањено изобличење тока. Квантитативне метрике перформанси, укључујући опоравак укупног притиска (TPR) и дисторзију протока (FD), процењене су коришћењем стандардних формулација. Генерално, студија потврђује ефикасност технике повратне спреге о притиску као пасивне стратегије управљања за побољшање оперативности и ефикасности надзвучних система за усис ваздуха под захтевним условима протока.